

A method for uniform demagnification imaging beyond the diffraction limit: cascaded planar hyperlens

Xing Tao · Changtao Wang · Zeyu Zhao ·
Yanqin Wang · Na Yao · Xiangang Luo

Received: 12 November 2012 / Accepted: 18 June 2013 / Published online: 4 July 2013
© Springer-Verlag Berlin Heidelberg 2013

Abstract Metamaterial composed of multistacked metal and dielectric films provides the access to ray tracing in subwavelength regions and to form a variety of transformation optical devices for manipulating light beyond the diffraction limit, such as hyperlens and cloak. In this paper, this method is employed to design planar hyperlens for demagnification imaging lithography. Variant ray route configurations are considered and compared for the sake of imaging quality as well as device structure complexity. It is found that specifically designed trajectory route from the object plane to the image plane help to yield imaging devices with uniform demagnification ratio and improved image quality. Then multiple similar imaging devices could be cascaded for further demagnification and reduce of structure complexity from the viewpoint of application. The imaging results with about $1/23$ wavelength (16 nm) half-pitch resolution in the measure of electric field intensity are demonstrated with numerical simulations. Also presented are the imaging characteristic analyses including light intensity, demagnification ratio and resolution.

1 Introduction

Conventional optics suffers from the so-called diffraction limit, because it is not capable of transmitting evanescent waves that carry subwavelength information about objects

[1]. To recover the evanescent waves, the concept of superlens constructed by one or multiple slabs of metal and dielectric material with matched permittivity is proposed [2–6]. Through the resonant coupling of evanescent waves to surface plasmons (SPs) at metal–dielectric interfaces, superlens could magnify evanescent waves and resultantly restore a subwavelength image. However, because these devices do not have magnification and demagnification capabilities, they always show their performance in the near field. Taking a form of cylindrical periodic stack of metal–dielectric multilayers, a hyperlens not only supports evanescent waves, but also achieves an image in magnification or demagnification manner [7–10]. One of the drawbacks of such a structure is that the input and output surface are curved profiles, which takes some trouble in locating objects as well as in measuring images. To avoid such problems, a conformal transformation theory is utilized to make planar input and output surfaces [11–13] with specially designed and complicated mathematic functions. But the demagnification ratio is not uniform on the entire input plane. Then, combining hyperlens with planar superlens and plasmonic reflector structure is proposed for improving imaging resolution and quality [14–16]. A simple way for planar imaging profile is to cut and polish hyperlens on one or both sides [17, 18]. But this operation seems challengeable for fabrication and usually delivers the deformation of images as can be seen in this paper.

In this letter, we present a design method of planar hyperlens for deep subwavelength imaging and uniform demagnification. Our design method is based on ray trajectories tracing of light on subwavelength scale in metamaterial constructed by alternatively stacked metal and dielectric films. By setting the ray trajectories of light between the object and image plane, we could build the surface profiles of multilayers inside the metamaterial.

X. Tao · C. Wang · Z. Zhao · Y. Wang · N. Yao · X. Luo (✉)
State Key Laboratory of Optical Technologies
on Nano-Fabrication and Micro-Engineering, Institute
of Optics and Electronics, Chinese Academy of Sciences,
P.O. Box 350, Chengdu 610209, China
e-mail: lxg@ioe.ac.cn

Numerical analyses indicate that the ray trajectories of piecewise cubic Hermite interpolating polynomial could realize uniform demagnification ratio, improved imaging quality, as well as simple device structures compared with ray trajectories of straight lines and some complicated curves. In addition, a larger demagnification ratio could be achieved by cascading multiple proposed hyperlenses, which provides further design freedom. Using this approach, an imaging result with about 1/23 wavelength half-pitch resolution is demonstrated with numerical simulations. Imaging characteristics such as contrast, demagnification ratio and electric field intensity are also analyzed.

2 Design principle

In order to guide waves to propagate along pre-determined trajectories in subwavelength regions between the planar input and output plane, a hyperbolic dispersion relation of metamaterial is employed. Given orthogonal coordinate curves (u , v , w) (as depicted in Fig. 1d), the hyperbolic dispersion relation for TM waves with magnetic field polarized along w -axis can be expressed as [11, 13].

$$k_u^2/\varepsilon_v + k_v^2/\varepsilon_u = (\omega/c)^2 \quad (1)$$

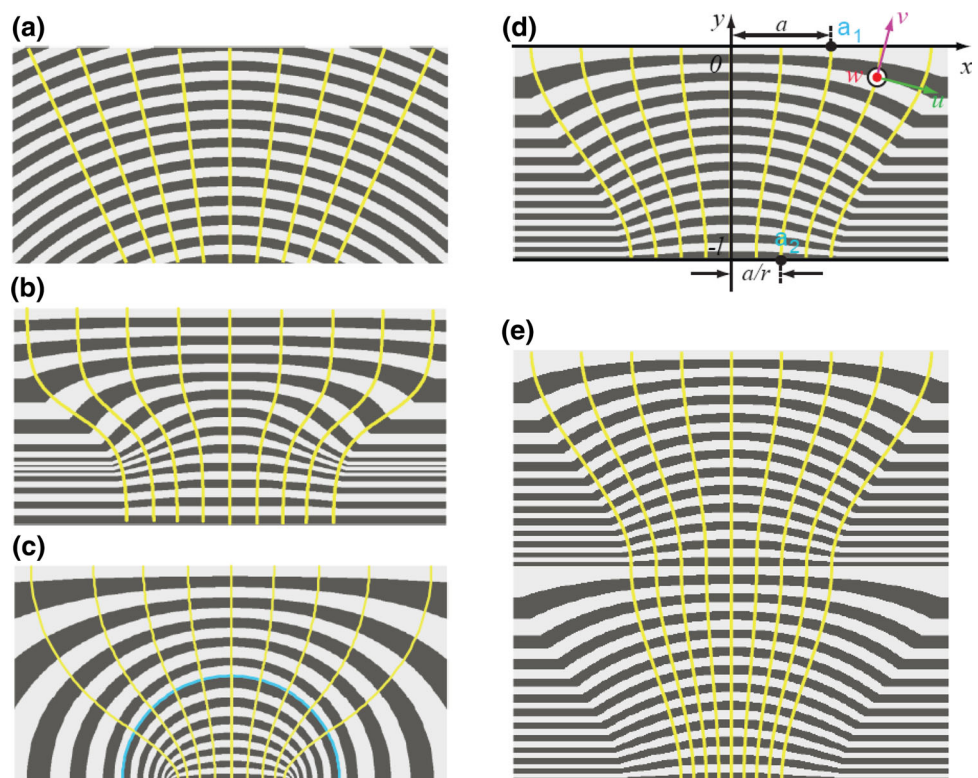
where ε_u and ε_v have opposite signs. According to the effective medium theory, ε_u and ε_v for anisotropic metamaterial built by the alternating metallic and dielectric

films are defined by the formula $\varepsilon_u \approx \varepsilon_d f_{\text{die}} + \varepsilon_m (1 - f_{\text{die}})$ and $\varepsilon_v \approx \varepsilon_d \varepsilon_m / (\varepsilon_m f_{\text{die}} + (1 - f_{\text{die}}) \varepsilon_d)$, in which f_{die} is the filling factor of dielectric films. Silver with $\varepsilon_{\text{Ag}} = -2.4012 + 0.2488i$ [8] and polymethyl-methacrylate (PMMA) with $\varepsilon_{\text{PMMA}} = 2.3013$ at the wavelength of 365 nm [3] are chosen for the alternating thin films. In our design, Ag and PMMA thickness are approximately equal, so $\varepsilon_u \approx (\varepsilon_{\text{Ag}} + \varepsilon_{\text{PMMA}})/2 = -0.0499 + 0.1244i$ and $\varepsilon_v \approx 2\varepsilon_{\text{Ag}}\varepsilon_{\text{PMMA}}/(\varepsilon_{\text{Ag}} + \varepsilon_{\text{PMMA}}) = 19.3232 + 36.6615i$. So the hyperbolic relation in Eq. (1) with opposite signs promises that light directional propagation along the v curves beyond the diffraction limit.

Figure 1 presents five configurations of planar hyperlenses that can realize demagnification image. The hyperlens shown in Fig. 1a is the conventional hyperlens with straight v curves. Note that the trajectories of electromagnetic waves are not perpendicular to the planar object and image plane. The v curves in Fig. 1b are constructed by the function $y = \ln(\tan(x))$. Although trajectories are approximately perpendicular to the planar surface, the thickness of layers varies greatly and the resolution and uniformity of images would be reduced. Moreover, the propagation direction changes rapidly in the hyperlens, and the coupling efficiency is low. The hyperlens structure demonstrated in Fig. 1c consists of two parts: The lower is an orthogonal oblate cylindrical system which enables imaging surface to be flat. The upper is an orthogonal system using conformal transformation from complex space to Cartesian coordinate

Fig. 1 Schematic of five types of planar hyperlens for planar demagnification image.

a Hyperlens with cylindrical geometry with straight v curves [17]. **b** Hyperlens where the v curves obey the function $y = \ln(\tan(x))$. **c** Hyperlens structure consists of two geometrical parts: The lower is an orthogonal oblate cylindrical system, and the upper is a multilayered hyperbolic structure as defined mathematically in Refs. [11, 13]. **d** Hyperlens of which the v curves are designed by piecewise cubic Hermite interpolating polynomial. **e** Cascading two proposed hyperlenses illustrated in **d**



to make the object surface planar. In this case, the complex structure is defined with complicated functions [11, 13]. Moreover, the demagnification ratio is not uniform on the entire input plane [11]. One optimum curvilinear orthogonal coordinate system (u, v, w) for the proposed planar hyperlens with demagnification ratio of r is presented in Fig. 1d. Assuming the length of the proposed hyperlens is l and the imaging point of $a_1(a, 0)$ on the object plane is $a_2(a/r, -l)$. The v curve connecting the two points can be determined by piecewise cubic Hermite interpolating polynomial (Fig. 1d), in which the slopes at the two end points are set to 0, that is

$$x(t) = (2t^3 - 3t^2 + 1)a/r + (-2t^3 + 3t^2)a, \tag{2}$$

where $t = (y + l)/l$. It is obviously that $t = 0$ and $t = 1$ refer to the output plane and input plane, respectively. This design method has three characteristics. (1) The v curves are perpendicular to the object and image planar surfaces when $y = 0$ and $y = -l$. (2) The demagnification ratio is exactly constant at any point on the object plane. The above two factors make it possible to get further demagnification by cascading multiple proposed hyperlenses without any distortions (Fig. 1e). (3) In addition, this method avoids any complicated mathematic functions as in Ref. [11] and could be easier to realize in practice.

3 Numerical simulations and discussion

3.1 Imaging behavior of a proposed hyperlens

As shown in Fig. 2, a normal plane wave with wavelength of 365 nm in TM-polarization illuminates from the top of the mask. The 50-nm-thick Cr mask (at 365 nm

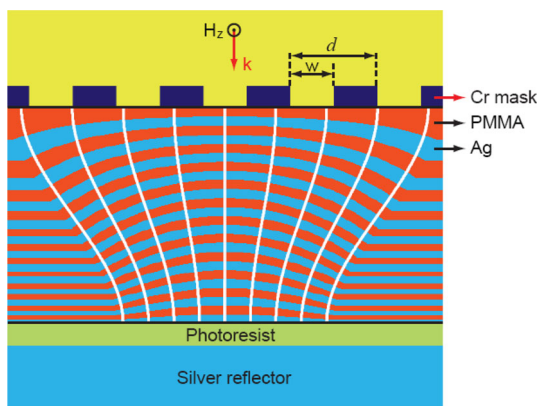


Fig. 2 The demagnification imaging lithography model with proposed hyperlens. All the components are treated as semi-infinite in z direction. Five slits are placed on the mask with slit width $W = 64$ nm and period $d = 128$ nm. The thickness of photoresist is 20 nm

wavelength $\epsilon_{Cr} = -8.55 + 8.96i$ [3]) has five equally spacing slits with 64 nm width and 128 nm period. The designed hyperlens below is filled by 25 pairs of silver/PMMA layers, each is about 20 nm thick. The smallest film thickness inside the ray tracing region is not smaller than 15 nm. It is worth to note that the feasible minimum silver film thickness for fabrication is about 15 nm or thinner, as reported in Refs. [19, 20]. The demagnification ratio is set as $r = 2$. A photoresist layer with 20 nm thickness and $\epsilon_{PR} = 2.56$ (ALLRESIST GMBH, Strausberg) is placed at the imaging plane. Below the resist is silver reflector layer acting as the plasmonic amplifier to improve imaging contrast [21, 22]. The thickness of the silver reflective layer is 60 nm, which is larger than the skin depth at 365 nm wavelength.

The simulation carried out by COMSOL Multiphysics 3.5 with finite element method shows that at the output surface, a pattern with 64 nm period is formed and the demagnification ratio is 2. Moreover, the electric field distributes uniformly along the y direction in the photoresist (Fig. 3a, inset). From the calculated $|E|^2$ field profile 10 nm below the output plane plotted by the solid red line in Fig. 3d, five lines with 32 nm width are obtained with intensity contrast

$$I = \left(|E|_{\max}^2 - |E|_{\min}^2 \right) / \left(|E|_{\max}^2 + |E|_{\min}^2 \right) \approx 0.61.$$

For comparison, the result of the control hyperlens of cylindrical geometry with straight v curves (Fig. 1a) is shown in Fig. 3c. The input and output plane are polished to plane [14]. The control hyperlens is designed to have the same demagnification ratio ($r = 2$), size and the number of metal-dielectric layers as the proposed one. Because the u curves have intersection points with the input plane, the trajectory of light for each slit passes different numbers of multilayers. This would lead to non-uniform field distribution on the imaging plane (shown in the inset of Fig. 3c), which greatly restricts the effective view region of the imaging device. In addition, strong surface plasmons are excited at the crossing points below the slits, which results in distortions of the waves propagating in the structure (white dashed line circles in Fig. 3c), and resultantly reduces the contrast. Meanwhile, the intersections between the u curves and the output plane will also result in strong light spots at the crossing points, and further reduce the contrast. In both designs, great light loss in silver films delivers considerably low efficiency of imaging field with intensity of about 0.03 normalized by the input light intensity. The light distribution for the control simulation shown as dashed line in Fig. 3d is not uniform with contrast of about 0.49, which is smaller than that of the proposed structure. Moreover, the inclination between the v curves and the output plane leads to oblique distribution of the electric field (see white rectangle shown in Fig. 3c

Fig. 3 **a** and **c** are the simulated electric field distributions ($|E|^2$) in the proposed hyperlens and control hyperlens, respectively. **b** The electric field distribution along the input plane. The period of the slits is 128 nm. **d** The electric field distribution on the plane 10 nm below the output plane. The *solid* and *dashed lines* refer to the proposed structure and control structure, respectively

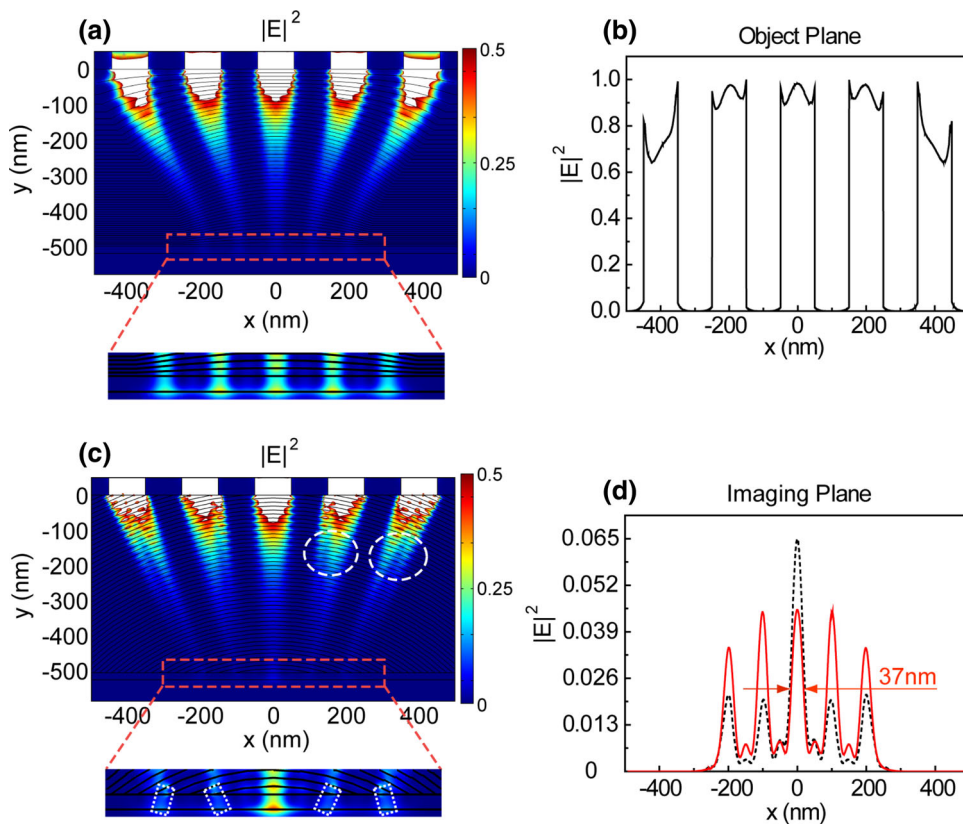
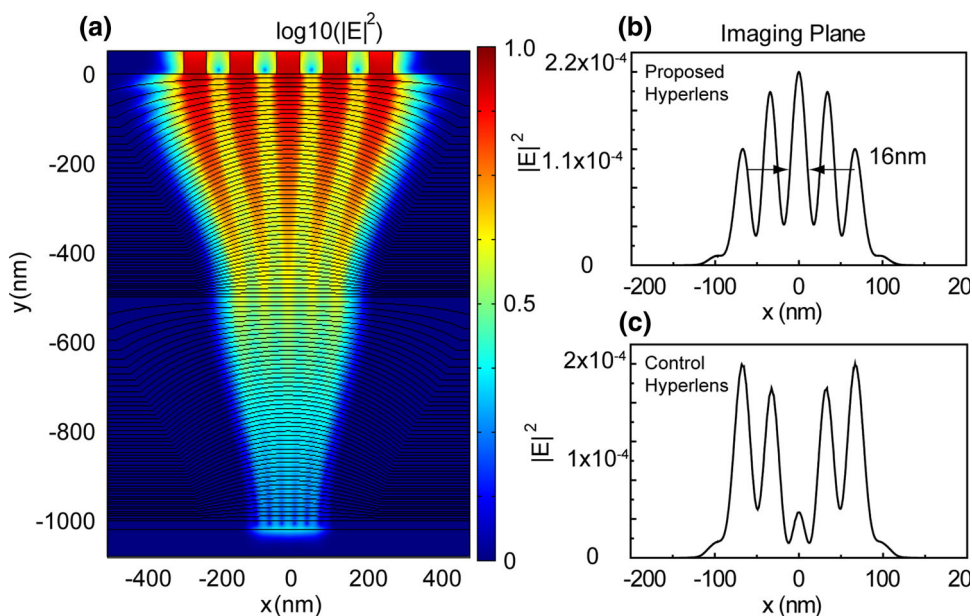


Fig. 4 **a** The simulated electric field distributions ($|E|^2$) in the cascaded hyperlens with mask same as Fig. 3. For better visualization, they are plotted in logarithm color scale. **b** and **c** are the electric field distributions on the plane 10 nm below the output plane for the proposed and control structures (Fig. 1a), respectively



inset) and resultantly reduces the uniformity of electric field distribution in the y direction in the photoresist layer.

3.2 Imaging behavior of two cascaded hyperlens

Next, we investigate the imaging performance of two cascaded hyperlens. Each hyperlens has a demagnification

ratio of 2, so that the 4 times demagnification ratio of the cascaded structure is expected. Since the v curves are perpendicular to the planar surface at the interface of the two hyperlens, light rays pass through the interface continuously and smoothly.

It is worth to note that, as can be seen from the calculated $|E|^2$ field profile in Fig. 4b, by introducing π phase

shift between adjacent slits, five equally spaced lines with half pitch of 16 nm (about $\lambda/23$) are obtained with contrast as high as 0.65. For comparison, the result of the cascaded control structure is shown in Fig. 4c. Because the layers could not be matched at the cascading interface, the middle slit is not resolved on the imaging plane. One obvious drawback of cascading two hyperlens with large magnification is that only slight light is transmitted through the hyperlens with normalized imaging field intensity of about 10^{-4} . This problem would not be a serious issue by

considering masks illumination with greatly focused light source.

In what follows, the uniform demagnification of position relationship between the object and imaging plane is demonstrated in Fig. 5. The simulation data agree well with the theoretical results. The maximum variations between the simulation data and the theoretical values are 1.2 nm ($\sim 0.3\%$) and 2.5 nm ($\sim 0.6\%$) for the single proposed hyperlens and the cascaded structure, respectively, which is mainly caused by the finite thickness of the metal and dielectric layers.

To investigate the imaging performance of our design structure, one slit is placed on the center of the mask and the FWHM of the electric field distribution on imaging plane is recorded in Fig. 6a. Restricted by the limit of resolution, the single proposed hyperlens and the cascaded structure exhibit the same focal spot size of about 23 nm when W is smaller than 40 nm. As W increases, the focal spot size for single hyperlens increases rapidly (from 22 nm when $W = 20$ to 49 nm when $W = 120$ nm) while the increment for the cascaded hyperlens is small (from 22 nm when $W = 20$ to 27 nm when $W = 120$ nm). As W increases from 20 to 120 nm, the electric field intensity at the focal spot on the imaging plane for single hyperlens reaches its maximum value when $W = 90$ nm while that of the cascaded hyperlens just increases smoothly (Fig. 6b).

Figure 7a demonstrates the slit width demagnification ratio for slits at different locations on the object plane. The

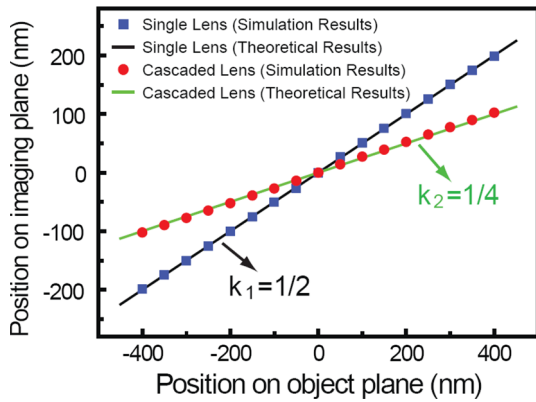


Fig. 5 The position relationship between the object and imaging plane indicates the demagnification characteristics of our devices. The lines are linear reduction relations of the theoretical results. The circle and rectangle are simulation data

Fig. 6 a FWHM of the electric field image distribution versus the slit width W for the proposed hyperlens (rectangle) and the cascaded structure of two proposed hyperlenses (circle), respectively. Only one slit opens on the center of the mask. **b** Normalized electric field intensity at the focal spot on the imaging plane versus the slit width W

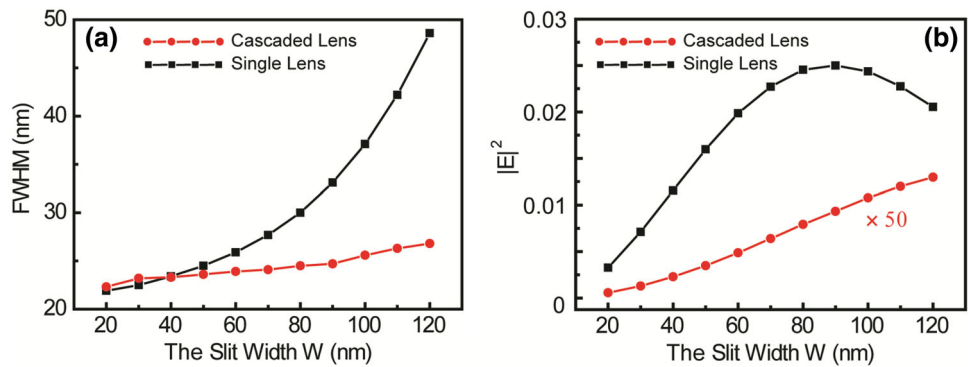
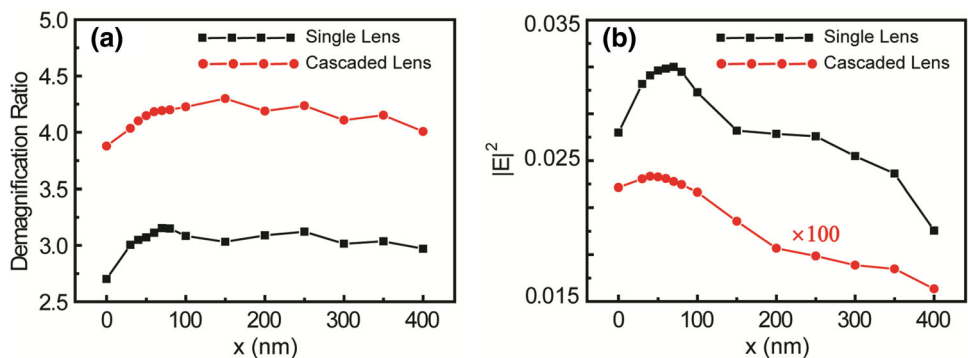


Fig. 7 a Demagnification ratio of the line width versus the position of the slit on the object plane for the proposed hyperlens (rectangle) and the cascaded two hyperlenses (circle), respectively. **b** Normalized electric field intensity at the focal spot on the imaging plane as a function of slit position



ratios between the maximum and minimum demagnification ratios along the x -axis are 1.16 and 1.10 for the single proposed hyperlens and the cascaded structure, respectively, indicating nearly uniform line width demagnification. The simulated electric field intensity at the focal spot on the imaging plane (Fig. 7b) reaches its maximum value when x equals 70 and 40 nm for the single proposed hyperlens and the cascaded structure, respectively, and then decreases monotonically as x further increases for both devices due to the increment of the optical path.

4 Conclusion

In summary, we demonstrate a design method of planar hyperlens that can achieve deep subwavelength imaging resolution. The geometry of the multilayered structure is determined by the proposed trajectory routes of piecewise cubic Hermite interpolating polynomial, which is perpendicular to both the input and output plane. In this way, the demagnification ratio is designed to be constant at any point on the object plane. Moreover, the designed planar hyperlens could be cascaded for further demagnification. Half-pitch resolution of about $1/23$ wavelength (16 nm) is obtained with the help of silver plasmonic reflector, and π phase shift associated with the mask. This method provides a simple and efficient way to achieve deep subwavelength resolution imaging, which is expected to be used in nanolithography, high-resolution microscope, optical storage device, etc.

Acknowledgments This work was supported by 973 Program of China (No. 2013CBA01700) and the Chinese Nature Science Grant (61138002, 61177013).

References

1. M. Born, E. Wolf, *Principles of Optics* (Cambridge University Press, London, 1999)
2. J.B. Pendry, *Phys. Rev. Lett.* **85**, 3966 (2000)
3. N. Fang, H. Lee, C. Sun, X. Zhang, *Science* **308**, 534 (2005)
4. D.O.S. Melville, R.J. Blaikie, *Opt. Express* **13**, 2127 (2005)
5. C. Wang, Y. Zhao, D. Gan, C. Du, X. Luo, *Opt. Express* **16**, 4217 (2008)
6. B. Wood, J.B. Pendry, D.P. Tsai, *Phys. Rev. B* **74**, 115116 (2006)
7. Z. Jacob, L.V. Alekseyev, E. Narimanov, *Opt. Express* **14**, 8247 (2006)
8. Z. Liu, H. Lee, Y. Xiong, C. Sun, X. Zhang, *Science* **315**, 1686 (2007)
9. H. Lee, Z. Liu, Y. Xiong, C. Sun, X. Zhang, *Opt. Express* **15**, 15886 (2007)
10. A. Salandrino, N. Engheta, *Phys. Rev. B* **74**, 075103 (2006)
11. W. Wang, H. Xing, L. Fang, Y. Liu, J. Ma, L. Lin, C. Wang, X. Luo, *Opt. Express* **16**, 21142 (2008)
12. W. Wang, L. Lin, X.F. Yang, J.H. Cui, C.L. Du, X.G. Luo, *Opt. Express* **16**, 8094 (2008)
13. S. Han, Y. Xiong, D. Genov, Z. Liu, G. Bartal, X. Zhang, *Nano Lett.* **8**, 4243 (2008)
14. H. Li, C. Wang, X. Luo, *Opt. Electron. Eng.* **38**, 35 (2011)
15. Y. Wang, B. Cheng, Y. Ho, Y. Lan et al., *Opt. Express* **20**, 22953 (2012)
16. G. Ren, C. Wang, G. Yi, X. Tao, X. Luo, *Plasmonics* **8**, 1065 (2013)
17. Y. Xiong, Z. Liu, X. Zhang, *Appl. Phys. Lett.* **94**, 203108 (2009)
18. J. Dong, J. Liu, X. Zhao, P. Liu et al., *Plasmonics*. (2013). doi: [10.1007/s11468-013-9570-6](https://doi.org/10.1007/s11468-013-9570-6)
19. Weiqiang Chen, Mark D. Thoreson, Satoshi Ishii, Alexander V. Kildishev, Vladimir M. Shalaev, *Opt. Express* **18**, 5124 (2010)
20. R. Chaturvedi, W. Wu, N.X. Fang et al., *Appl. Phys. Lett.* **96**, 043102 (2010)
21. M.D. Arnold, R.J. Blaikie, *Opt. Express* **15**, 11542 (2007)
22. X. Yang, L. Fang, B. Zeng, C. Wang, Q. Feng, X. Luo, *J. Opt.* **12**, 045001 (2010)